Journal of Orthopaedic Translation 36 (2022) 64–74

Contents lists available at ScienceDirect

Journal of Orthopaedic Translation

journal homepage: www.journals.elsevier.com/journal-of-orthopaedic-translation

Differential dynamics of bone graft transplantation and mesenchymal stem cell therapy during bone defect healing in a murine critical size defect

Elijah Ejun Huang [a,1], Ning Zhang [a,1], Edward A. Ganio [b], Huaishuang Shen [a], Xueping Li [a], Masaya Ueno [a], Takeshi Utsunomiya [a], Masahiro Maruyama [a], Qi Gao [a], Ni Su [a], Zhenyu Yao [a], Fan Yang [a,c], Brice Gaudillière [b], Stuart B. Goodman [a,c,*]

[a] Department of Orthopaedic Surgery, Stanford University, Stanford, CA, USA
[b] Department of Anesthesiology, Perioperative and Pain Medicine, Stanford University, Stanford, CA, USA
[c] Department of Bioengineering, Stanford University, Stanford, CA, USA

ARTICLE INFO

Keywords:
Bone graft
Critical-size bone defect
CyTOF
Macrophages
Stem cells
T cells

ABSTRACT

Background: A critical size bone defect is a clinical scenario in which bone is lost or excised due to trauma, infection, tumor, or other causes, and cannot completely heal spontaneously. The most common treatment for this condition is autologous bone grafting to the defect site. However, autologous bone graft is often insufficient in quantity or quality for transplantation to these large defects. Recently, tissue engineering methods using mesenchymal stem cells (MSCs) have been proposed as an alternative treatment. However, the underlying biological principles and optimal techniques for tissue regeneration of bone using stem cell therapy have not been completely elucidated.

Methods: In this study, we compare the early cellular dynamics of healing between bone graft transplantation and MSC therapy in a murine chronic femoral critical-size bone defect. We employ high-dimensional mass cytometry to provide a comprehensive view of the differences in cell composition, stem cell functionality, and immunomodulatory activity between these two treatment methods one week after transplantation.

Results: We reveal distinct cell compositions among tissues from bone defect sites compared with original bone graft, show active recruitment of MSCs to the bone defect sites, and demonstrate the phenotypic diversity of macrophages and T cells in each group that may affect the clinical outcome.

Conclusion: Our results provide critical data and future directions on the use of MSCs for treating critical size defects to regenerate bone.

Translational Potential of this article: This study showed systematic comparisons of the cellular and immunomodulatory profiles among different interventions to improve the healing of the critical-size bone defect. The results provided potential strategies for designing robust therapeutic interventions for the unmet clinical need of treating critical-size bone defects.

1. Introduction

Approximately 6.3 million cases of fractures of bone occur every year in the United States. In about 100,000 of these cases, bone is lost or excised, and the remaining gap is too large to heal spontaneously [1]. In this scenario, the non-union will persist as a "critical-size bone defect" without surgical intervention.

The current treatment for such defects is the use of autologous bone grafting to the local defect to facilitate bone healing. However, bone graft is limited in quality and quantity, and harvesting of bone increases the risk of infection and may result in persistent local pain and disability [2,3]. Recently, the principles of tissue engineering, regenerative medicine, and cell therapy have been considered as techniques to improve healing of bone defects and avoid the use of autologous bone graft. MSCs are the precursors of osteoblastic lineage cells and are capable of regenerating bone, cartilage, fibrous tissue, skeletal muscle, and many other mesenchymal tissues [4–8]. Other elements including a scaffold, growth factors and other molecules are combined with progenitor cells to provide the

* Corresponding author. Department of Orthopaedic Surgery, Stanford University, Stanford, CA, USA.
E-mail address: goodbone@stanford.edu (S.B. Goodman).
[1] These authors contributed equally to this work

https://doi.org/10.1016/j.jot.2022.05.010
Received 6 March 2022; Received in revised form 22 May 2022; Accepted 27 May 2022

necessary components for osteogenesis [9]. However, MSC lineage cells are not the only cell subset participating in bone healing, macrophages, dendritic cells, T cells have all been reported to engage in crosstalk with MSCs and contribute to the bone healing process [10–15]. Additionally, there is limited information concerning the exact cellular constituents and complex crosstalk among different cell populations that direct the process of bone healing. Thus, stem cell therapy has yet to be optimized.

To bridge the gap of knowledge in this area, our overall goal in this study is two-fold: first, to elucidate the profiles of the different cell populations and signaling molecules participating in the early stages of bone-graft-associated healing; second, to compare the biological profiles of bone graft transplantation and MSC-based cell therapy early in the healing process.

To achieve these goals, we have employed high-dimensional Cytometry by Time Of Flight mass spectrometry (CyTOF) to analyze samples collected from mice with critical-size bone defects one week after grafting. By measuring over 40 cell-surface and intracellular proteomic markers per cell, we provided a comprehensive view of cell composition, functionality, and immunomodulatory activity between bone graft transplantation and the MSC based therapy. This result will help guide the development of novel biological constructs that mimic the performance of bone graft for treating critical-size bone defects.

2. Materials and methods

2.1. Isolation of MSCs

Bone marrow-derived MSCs were isolated from male BALB/c mice and characterized as previously described [16]. Briefly, 8- to 10-week-old BALB/c male mice were used to collect the bone marrow from femurs and tibias. The bone marrow with cells was filtered through a 70 μm cell strainer, spun down and resuspended using α-minimal essential medium (α-MEM, Thermo Fisher Scientific, Waltham, MA USA) supplied with 10% certified fetal bovine serum (FBS, Invitrogen, Thermo Fisher Scientific, Waltham, MA USA) and antibiotic-antimycotic solution (100 units of penicillin, 100 μg of streptomycin and 0.25 μg of amphotericin B per milliliter, Hyclone, Thermo Fisher Scientific, Waltham, MA USA). Unattached cells were removed by replacing medium the next day (passage 1). Flow cytometry (LSRII, Stanford Shared FACS Facility) was used to characterize the immunophenotype of isolated MSCs at passage 4: spinocerebellar ataxia type 1 (Sca1+)/CD105+/CD44+/CD34-/CD45-/CD11b-. Identified MSCs at passage 4–8 were used in the experiments. This protocol has been approved by Stanford's Administrative Panel on Laboratory Animal Care (APLAC) (#APLAC-9964).

2.2. Generation of genetically modified MSCs

The lentiviral vector preparation was performed as previously described [17,18]. Human embryonic kidney 293T cells (ATCC, Manassas, VA, USA) were used to transfect the green fluorescent protein (GFP) expressing lentivirus vector pCDH-CMV-MCS-EF1-copGFP together with the psPAX2 packaging vector, and pMD2G VSV-G envelope vector using a calcium phosphate transfection kit (Clontech, Mountain View, CA, USA) with 25 μM chloroquine. Titer of the harvested virus was detected 48 h after the transfection. The virus was diluted in MSC culture medium supplemented with 10 μg/mL of polybrene (Sigma Aldrich, St. Louis, MO, USA), and used to infect murine MSCs at multiplicity of infection (MOI) = 100. At 3 days post-infection, the infected cells were confirmed as GFP positive by fluorescence microscopy (Keyence, Itasca, IL, USA) (Fig. 1B, left).

2.3. Critical-size bone defect murine model

Eight-week old wild-type BALB/cByJ mice were purchased from the Jackson Laboratory (Bar Harbor, ME, USA). APLAC approved this animal experiment protocol (#APLAC-26905) Stanford University's guidelines for the care and use of laboratory animals were strictly followed. Subcutaneously injection of 0.1 mg/kg of buprenorphine was given to the mice for preoperative analgesia. While under 2–3% isoflurane in 100% oxygen inhalation anesthesia, right sided 2 mm critical sized femoral defects were made in the mice using a special jig; the femur was stabilized with a custom murine external fixator (Fig. 1A) [9,19,20]. Our previous studies [9,20,21] showed that the 2-mm defect would not heal spontaneously 6 weeks after establishment of the defect without interventions. Accordingly, a 2 mm bone defect size was used in the current study. Four weeks after the critical size defect was established, the secondary surgeries were performed to transplant bone graft or scaffold with cells into the bone defect site.

2.4. Bone graft harvest and transplantation

The mice designated as bone graft donors were eight-week old gene-modified CD90.1 BALB/cByJ mice and were a gift from the Negrin Lab at Stanford University [21]. In comparison, the wild-type BALB/cByJ mice

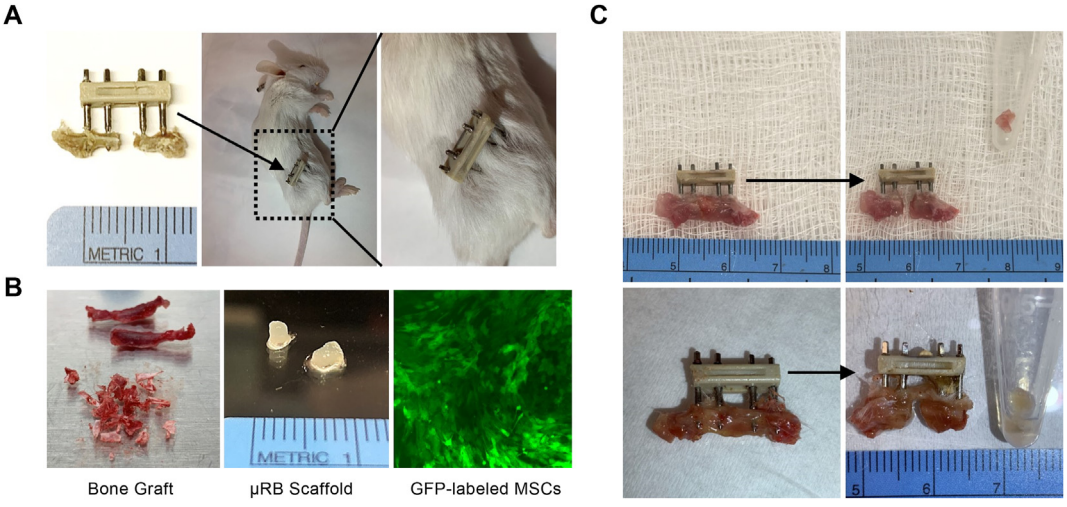

Fig. 1. Murine critical-size bone defect model and sample collections from bone defect sites. A) 2 mm critical-sized defect has been created in the mouse femur and stabilized with an external fixation device. B) Bone graft harvested from iliac crest (left) and microribbon (μRB) scaffold (middle) embedded with GFP-labeled MSCs (right) are ready for transplantation. C) Tissue samples containing bone graft (top panel) or μRB scaffold (bottom panel) collected from bone defect sites.

receiving bone graft transplantation express CD90.2, and thus, cells from donor mice and from recipient mice could be distinguished using these two different isotypes of CD90. On the same day immediately before the secondary surgeries, the bone graft was harvested from the iliac crest of the donor mice (Fig. 1B, left) and then transplanted to fill the bone defect sites of the recipient mice. While most of the iliac crest bone graft from donor mice was transplanted into recipient mice, the remaining excess iliac crest bone was collected and analyzed separately. One week after the secondary surgeries, the entire tissue within the bone defect site was harvested for analysis (Fig. 1C, top panel).

2.5. MSCembedded scaffold preparation and implantation

Gelatin micron-ribbon scaffolds (μRBs) were fabricated through a wet spinning process according to a previous report [22,23]. To fabricate scaffolds and embed MSCs within them, the μRBs were rehydrated in PBS containing 0.05% LAP photo-initiator. After 1 h of incubation at 37C, trypsinized MSCs suspended in PBS were gently mixed with the μRBs. The final uRB concentration is 7.5% (wt%) with 10 million cells/ml. The cell-containing μRBs were placed into cylindrical molds with diameter of 2 mm and height of 2 mm and exposed to ultraviolet light (365 nm, 2 mW/cm2) for 4 min to produce macroporous scaffolds. The scaffolds were then gently pushed out from the mold and kept in culture medium containing 10% FBS one day prior to the secondary surgeries (Fig. 1B, middle). During the secondary surgeries, the 2 mm long μRB scaffolds embedded with GFP-labeled MSCs were implanted into the bone defect site. One week after the secondary surgeries, the entire tissue within the bone defect site was harvested for analysis (Fig. 1C, bottom panel).

2.6. Cytometry by Time Of Flight (CyTOF)

The tissues harvested from the bone defect site were first dissociated into single cells and then fixed in 2% PFA. Once all samples were collected and fixed, cells were analyzed using high-dimensional mass cytometry (also known as Cytometry by Time Of Flight or CyTOF). Cells were barcoded, permeabilized, and stained with a cocktail of antibodies tagged with metal isotopes according to a standardized protocol [24–26]. Stained cells were then washed and re-suspended in MilliQ water and analyzed using the Helios mass cytometry platform (Fluidigm, Inc., South San Francisco, CA) (Figure S1-A). A panel of 40 antibodies mediators (Supplementary Table 1) was used to identify specific cell types and multiple relevant signaling pathway. Antibodies were purchased pre-conjugated from Fluidigm or were conjugated in-house to purified, carrier-free stocks from Biolegend (http://www.biolegend.com) and Abcam (http://www.abcam.com).

2.7. Study cohort

This study consists of 3 cohorts of mice. The respective procedures for each cohort are described as follows.

For the first cohort (Fig. 2, top panel), surgeries were performed on 6 mice. After 5 weeks, the tissue within the bone defect sites was collected. Since there were no transplantations performed in this cohort, the amount of the tissue collected within the bone defect sites was limited. Thus, tissue collected from all 6 mice was pooled into one sample for CyTOF analysis, from which only 1400 cells were obtained. This is the "Bone Defect (BD) Tissue Empty Ctrl" group.

For the second cohort (Fig. 2, middle panel), primary surgeries were performed on 8 mice. After 4 weeks, secondary surgeries were performed to transplant the μRB scaffolds embedded with GFP-labeled MSCs into the bone defect sites. After another week (5 weeks after the primary surgeries), the tissues within the bone defect sites containing the MSC-μRB scaffold transplants were collected. Since there was insufficient yield of cells from the digestion process of the μRB scaffolds, tissues collected from 8 mice in this cohort were pooled into 4 samples for CyTOF, resulting in about 150,000 cells from each sample. This is the "BD Tissue w Scaffold + MSC" group.

For the third cohort (Fig. 2, bottom panel), primary surgeries were performed on 8 mice. After 4 weeks, secondary surgeries were performed to transplant the iliac crest bone graft from the donor mice to the bone defect sites of the recipient mice. After another 1 week (5 weeks after the primary surgeries), the tissues within the bone defect sites containing the bone graft transplants from these 8 mice were collected for CyTOF, resulting in about 80,000 cells from each sample. This is the "BD Tissue w Bone Graft" group.

The remaining iliac crest bone (bone graft resource) from 8 donor

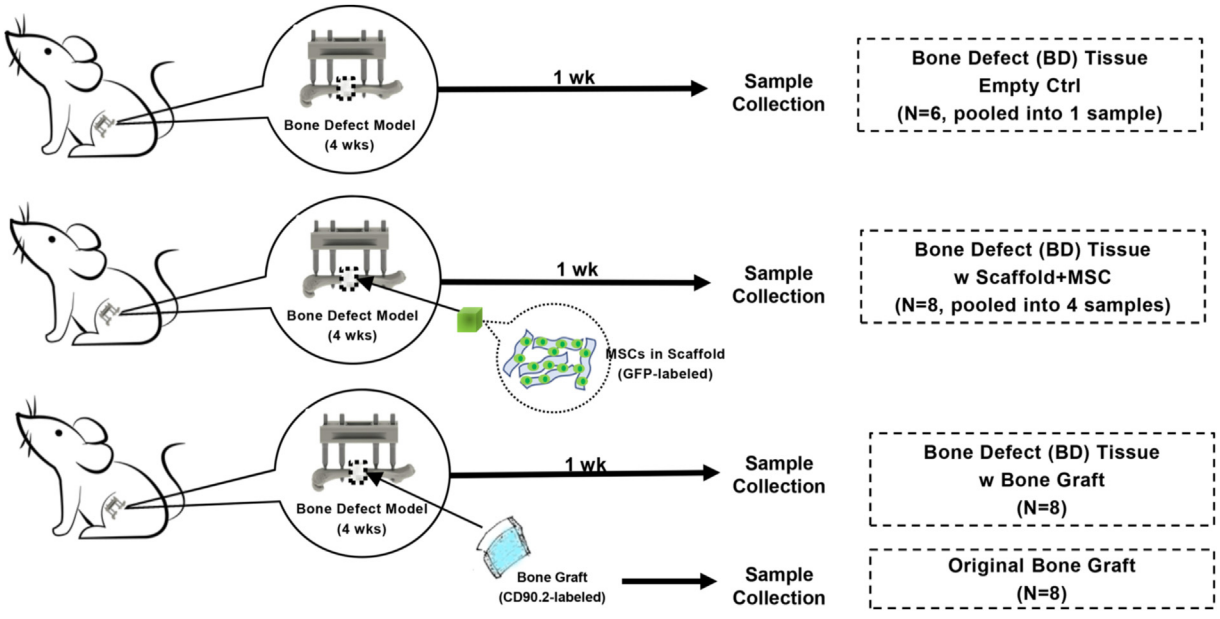

Fig. 2. Diagram of experimental design and bone defect model in mice. In each experiment, we first applied the external fixation device onto the left femur, created the 2 mm femoral midshaft diaphyseal bone defect, closed the wound, applied various treatments 4 weeks later after the nonunion was established, and then subsequently harvested the tissue in the defect 1 week later.

mice was collected to demonstrate the cell composition of the original bone graft and about 250,000 cells from each sample were obtained for data analysis. This is the "Original Bone Graft" group.

2.8. Data analysis

The raw data obtained from CyTOF were normalized and de-barcoded, then uploaded onto the cloud-based computational tool, Cytobank (http://www.cytobank.com), for both cell subset-specific gating and multiparametric analysis (viSNE, FlowSOM). A universal data cleaning process was performed on all samples to remove debris, doublets, dead cells, and red blood cells (RBCs) for each sample (Figure S1-B). After data cleaning, a universal gating strategy was applied using multiple phenotypical markers to identify major cell types (Figure S2). Briefly, CD45 was first used to distinguish leukocytes from non-leukocytes. Within the leukocyte population, Ly6G was used to separate granulocytes and mononuclear cells. Among mononuclear cells, CD3 was used for identifying T cells, CD19 for B cells, CD49b for NK cells, CD11c for dendritic cells (DCs), and CD11b plus F4/80 for macrophages. Within the non-leukocyte population, CD31, Sox9, and Pax7 were used to reveal endothelial cells, chondrocytes, and muscle satellite cells, respectively. The cell count of a specific cell type is compared with the cell count of the single, live, non-RBCs (i.e., total cell population) to determine the percentage of this specific cell type within the total cell population. Significant changes between different samples are determined by one-way ANOVA using PRISM GraphPad with a two-sided level of significance of $\alpha = 0.05$.

3. Results

Distinct Cell Compositions among Tissues Collected from Bone Defect Sites, Reflecting the Different Clinical Outcomes between the Bone Graft Transplantation and MSC Therapy.

We identified the major cell populations using a traditional gating strategy (Figure S2 and described in "Materials and Methods") and compared their frequencies among the 4 groups (Fig. 3A). Only 1400 cells were obtained for the "BD Tissue Empty Ctrl" group from all 6 mice. This low yield of cells indicated very limited cellular activities occurring within the bone defect site and suggested that the gap would not heal spontaneously without surgical intervention. Due to this low yield, no statistical analysis could be performed for this group and only a few major cell populations could be identified with confidence.

As expected, granulocytes ($CD45^+$, $Ly6G^+$) are the major cell population (~62%) in the "Original Bone Graft" group (Fig. 3A); this is expected since they emanate from the bone marrow [27]. In all three groups with chronic bone defect, granulocytes are not a major population and only accounted for ~10% or less of cells. The most abundant type of granulocytes is neutrophils, which are regarded as the first-line responder to the early stages of inflammation and set the stage for macrophages to repair tissue damage [27,28]. The presence of neutrophils indicates the occurrence of early-stage immune response within the bone defect sites. The "BD Tissue w Scaffold + MSC" group contained significantly more neutrophils compared with "BD Tissue w Bone Graft" group (~9% vs ~3%), which might indicate that using scaffold plus exogenous MSCs as transplants may have delayed the transition from the acute to the repair stage of bone healing.

Next, we examined the monocyte-derived cells, including macrophages ($CD45^+$, Ly6G-, $CD11b^+$, $F4/80^+$) and DCs ($CD45^+$ $Ly6G^-$, $CD11c^+$). Macrophages are involved in all stages of fracture healing and have a major impact on long-term bone regeneration [29,30]. They comprised about 10% of the total cell population. DCs are one major type of antigen-presenting cells (APCs) and are responsible for the initiation of the adaptive immune response [31]. DCs can also act in conjunction with osteoclast precursors to modulate bone destruction [32]. We observed a higher percentage of DCs in the "BD Tissue w Scaffold + MSC" group compared with the "BD Tissue w Bone Graft" group (3.0% vs 1.8%), which may correlate with the inferior bone healing when using Scaffold plus MSCs as bone transplants.

The lymphocyte population consisted of B cells ($CD45^+$, $Ly6G^-$, $CD19^+$), T cells ($CD45^+$, $Ly6G^-$, $CD3^+$), and NK cells ($CD45^+$, $Ly6G^-$, $CD49b^+$). There were significantly more B cells in the "BD Tissue w Scaffold + MSC" group (~11%) compared with the "BD Tissue w Bone Graft" group or the "Original Bone Graft" group (both below 1%). T cells comprise a major population in the "BD Tissue w Scaffold + MSC" group (~24%), but in the "BD Tissue w Bone Graft" group, the percentage of T cells varied from 1% to 40%. B cells and T cells participate in initial fracture repair by infiltrating the callus in two waves, first accumulating at the fracture site on Day 3, decreasing by Day 7, and then re-entering the callus after Day 14 [33]. Since the current model is a chronic critical-size bone defect similar to a nonunion, on Day 7, the behaviors of B cells and T cells might not parallel the scenario of an acute bone fracture. However, this dramatic difference in the percentages of B and T cells among these two groups of bone defect tissues might reflect the temporal variations in transitioning from a pro-inflammatory state to an anti-inflammatory state induced by either the scaffold plus MSCs or by the bone graft. Although NK cells are reported to interact with MSCs and thus, play an important role in regulating bone regeneration [34,35], few NK cells were detected in all our study groups, casting doubt on their importance in bone healing within the critical size bone defect model.

We also quantified the non-leukocyte ($CD45^-$) population, including chondrocytes ($CD45^-$, $Sox9^+$), endothelial cells ($CD45^-$, $CD31^+$), and muscle satellite cells ($CD45^-$, $Pax7^+$). Chondrocytes were not detected in any of the samples, which is similar to our previous studies using this model [9,36,37]. Very few endothelial cells and muscle satellite cells were detected on Day 7.

To complement the analysis of traditionally gated cell subsets, which depends on prior knowledge of cell phenotypes, we employed an unsupervised dimension reduction algorithm (viSNE) to generate a holistic view of overall cell composition. The "BD Tissue Empty Ctrl" group was not included in all multiparametric analyses (viSNE, FlowSOM) due to insufficient cell numbers.

We first colored the viSNE plot according to the expression levels of individual phenotypic biomarker (selected ones are shown in Fig. 3B) and visualized distinct cell clusters that corresponded to major cell population. For example, the cell cluster on the right-side showed high expression of CD45, Ly6G, and CD11b, and low expression of CD3, CD19, MHCII, and CD11c; thus, this cell cluster represents granulocytes. Using this method, we identified the most common cell types on the plot for all 3 groups.

Next, we colored the viSNE plot by gated cell population to show the landscapes of overall cell composition for each group (Fig. 3C). We found that the total cell populations from all groups consisted of 4 major cell types. The first cell population located on the top of the plot is non-leukocytes (shown in light gray), which contains identifiable numbers of MSCs (shown in dark red). The second cell population located on the right-side represents granulocytes (shown in orange). The third cell population located at the bottom is T cells (shown in cyan). The fourth cell population is antigen-presenting cells (APCs), which includes a cluster of B cells on the left-side (shown in green), a cluster of macrophages in the middle (shown in pink), and a few DCs and other APCs scattered in between. Clearly, the overall landscapes of cell composition are distinctive across these 3 groups.

We further quantified the percentages of these 4 major cell types to visualize the differences in the 3 groups (Fig. 3D) and color-coded the columns corresponding to the cell populations in Fig. 3C. In the "Original Bone Graft" group that shows the original state of the bone graft (bone marrow), ~61% of the cells are granulocytes and the remaining ~34% of the cells are mostly monocytes and macrophages (one type of APCs). T cells and other non-leukocytes are uncommon and consist only 5% in this group. When comparing the cell compositions of the other two groups, we observe more granulocytes and APCs, a similar ratio of T cells, and less non-leukocytes in the "BD Tissue w Scaffold + MSC" group, which

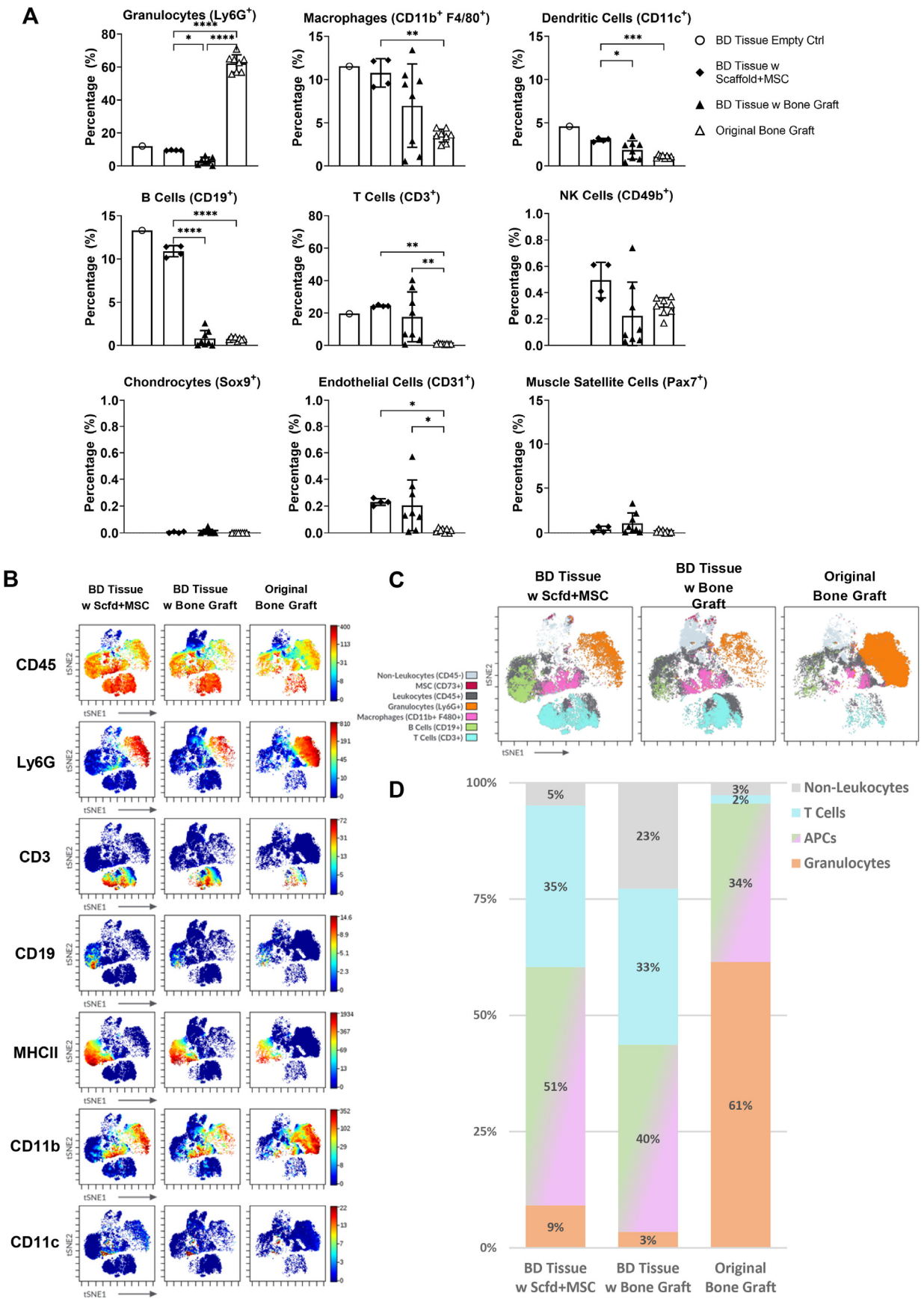

Fig. 3. Distinct cell compositions among tissues from bone defect sites compared with original bone graft. A) Frequency of major cell subsets. B) viSNE plots colored according to phenotypic marker expression. C) viSNE plots depicting major cell populations identified based on phenotypic marker expression. D) The frequency of cell populations depicted in C was quantified.

appears to indicate higher inflammatory activity at the bone defect sites transplanted with scaffold plus MSCs, compared with those transplanted with bone graft.

Active Recruitment of MSCs to the Bone Defect Sites, Suggesting Bone Healing Process is Triggered by Transplants but Primarily Conducted by Autologous Cells.

Previous studies have suggested that crosstalk among different types of cells may collectively contribute to the bone healing process [36–39]. We therefore sought to elucidate cell compositions in tissues from bone defect sites that contained either the MSCs-embedded scaffold or the bone graft and compare them with that of the original bone graft.

MSCs have been shown to play a crucial role in bone healing [38–40]. Therefore, multiple biomarkers (including $CD45^-$, $CD31^-$, $Sca1^+$, $CD44^+$) for the identification of MSCs were included in this analysis. We found there are significant more MSCs within the bone defect tissues, either implanted with scaffold plus MSCs or with bone graft, compared with the original bone graft (Fig. 4A). We identified the MSCs population ($CD45^-$, $CD31^-$, $Sca1^+$, $CD44^+$) and compared their percentages versus total population and versus non-leukocytes population (Fig. 4B).

We identified about 0.03% of the total population (about 100 cells in each sample) as MSCs in the "Original Bone Graft" group, which agrees with previous reports regarding the percentages of MSCs in bone marrow [41,42]. In the "BD Tissue w Bone Graft" group, about 0.8% of the total population are MSCs. Given that the MSC percentage is very low (~0.03%) in the original bone graft, this large number of MSCs (~0.8%) indicates either an active recruitment of MSCs to the bone defect sites, a significant proliferation of the implanted MSCs, or a combination of both (Fig. 4B, left). MSCs account for about 1.7% of the total population in the "BD Tissue w Scaffold + MSC" group. This percentage of MSCs is expected to be high, since we embedded MSCs into the scaffolds before transplanting them into bone defect sites.

In addition, a higher proportion of non-leukocytes was observed in the "BD Tissue w Bone Graft" group (~23%) compared with the "BD Tissue w Scaffold + MSC" group (~5%) or the "Original Bone Graft" group (~3%) (Fig. 3D). As the frequency of MSCs may be heavily impacted by the abundance of the leukocytes versus non-leukocytes, we also examined the percentage of MSCs within the non-leukocyte population (Fig. 4B, right). We found about 36% of the non-leukocytes are MSCs in the "BD Tissue w Scaffold + MSC" group, but in the "BD Tissue w Bone Graft" group, only 5% of the non-leukocytes are MSCs. This suggests that the "BD Tissue w Scaffold + MSC" group is associated with active local recruitment of local MSCs and/or MSC proliferation.

We further explored the origins of the MSCs accumulated at the bone defect sites. They were either recruited to the bone defect sites from the host mouse (recruited MSCs) or derived from the MSCs which originally resided within the scaffold or bone graft (implanted MSCs). The MSCs embedded within the scaffolds are genetically modified GFP-labeled MSCs, therefore we included an anti-GFP antibody to distinguish these GFP-labeled MSCs (Fig. 4C, left). To distinguish the MSCs from host mice versus from the bone graft of the donor mice, we included the biomarker CD90.2 (Thy1.2). CD90 is a biomarker that is primarily expressed in T cells and stem cells (such as MSCs) and has two isotypes: CD90.1 and CD90.2. In our experimental design, the donor mice express CD90.1 and the host mice express CD90.2. By detecting CD90.2 expression, both MSCs and T cells can be distinguished from donor and host mice (Fig. 4C, right). Taking advantage of both GFP and CD90.2 biomarkers, we found that the majority of the MSCs were recruited to the bone defect sites from the host mice instead of derived from the implanted MSCs. This active recruitment of MSCs was observed both in the "BD Tissue w Scaffold + MSC" group (72% are recruited MSCs) and in the "BD Tissue w Bone Graft" group (64% are recruited MSCs) (Fig. 4D).

3.1. *Macrophages population shows increased phenotypic diversity in the bone defect tissues, indicating active immune response at early stage of bone healing*

Macrophages have a major immunomodulatory effect during the bone healing process [43]. We first identified the macrophage population ($CD45^+$, $Ly6G^-$, $CD11b^+$, $F4/80^+$) and within macrophages, we further examined their subtypes, which are often categorized as M0 (uncommitted), M1 (pro-inflammatory), and M2 (anti-inflammatory pro-reconstructive) [44–46]. M2 macrophages have been subdivided into M2a, M2b, M2c, and M2d [47,48]. There are many biomarkers that have been reported to differentiate M1 and M2 macrophages. CD80, CD86, MHCII, and iNOS have commonly been regarded as M1 macrophage markers, while CD206, CD163, and Arg-1 have commonly been regarded as M2 macrophage markers [45,46,49]. However, these categorizations remain controversial due to the lack of universal criteria to define each subtype. For example, CD86 and MHCII have been reported to be expressed on M2b macrophages [48–50] and iNOS has been reported to

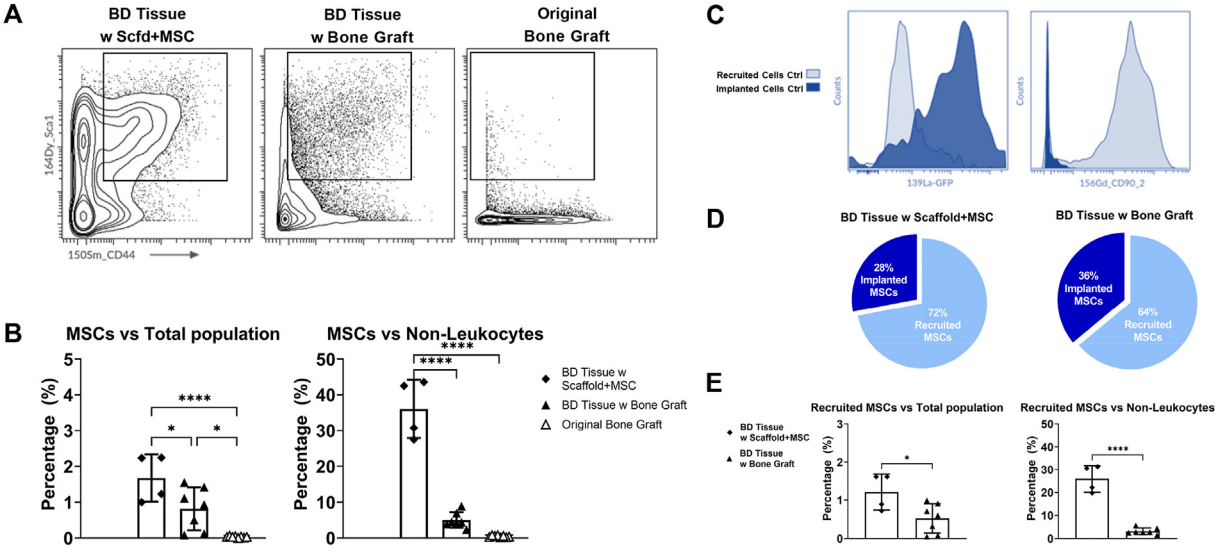

Fig. 4. Active Recruitment of MSCs to the Bone Defect Sites. A) Contour plots of MSCs population (Sca1+, CD44+) in 3 groups. B) Quantification of MSCs percentages versus total population and versus non-leukocytes. C) Validation of GFP and CD90.2 as biomarkers to distinguish recruited cells and implanted cells. D) Proportions of recruited MSCs versus implanted MSCs in 2 groups of bone defect tissues. E) Quantification of recruited MSCs percentages versus total population and versus non-leukocytes.

be expressed on M2d macrophages [49]. In our study, M0 macrophages were identified as $CD11b^{+}$ $F4/80^{+}$ $MHCII^{-}$ $CD206^{-}$ cells, M1 macrophages were identified as $MHCII^{+}$ $CD206^{-}$ cells, and M2 macrophages were identified as $MHC^{+/-}$ $CD206^{+}$ cells.

We examined the percentages of M0, M1, and M2 macrophages versus the pan-macrophage population or the total population (Fig. 5A, left). In the "Original Bone Graft" group, the majority of macrophages (~88%) were M0. In the other 3 groups, the proportion of M0 macrophages was significantly decreased, indicating macrophages had been polarized to the M1 or M2 phenotype at the bone defect sites. M1 macrophages only consisted of about 10% of the macrophage population in the "Original Bone Graft" group but increases to 20%–30% in all three groups of bone defect tissues, suggesting increased inflammation at the bone defect sites. In the "Original Bone Graft" group, M2 macrophages are hardly detectable (<1%). However, in the "BD Tissue w Bone Graft" group, the proportion of M2 macrophages increased to 8%. In the "BD Tissue w Scaffold + MSC" group, the proportion of M2 macrophages even increased to 40%, which is similar to the "BD Tissue Empty Ctrl" group (~32%). This suggests that one week after the second surgeries, the immunomodulatory effects of the transplanted MSCs in the "BD Tissue w Scaffold + MSC" group have transitioned the local microenvironment to an anti-inflammatory stage, while the bone defect site containing iliac crest bone graft remained at the pro-inflammatory stage. This observation is consistent with the fact that MSCs promote macrophages to polarize towards an M2 phenotype [51]. Since the proportions of macrophages in the total cell population are not significantly different among these three groups (Fig. 3A, top-middle), similar trends were also observed when we examined the percentages of M0, M1, and M2 macrophages versus total population (Fig. 5A, right).

Classifying macrophages into M1 and M2 phenotypes is an oversimplification and does not adequately reflect the phenotypic diversity of the macrophage cell compartment. To fully reveal the spectrum of macrophage populations, we performed an unsupervised FlowSOM analysis of the macrophage population identified using viSNE (Fig. 5B). FlowSOM considers a full panel of biomarkers holistically to parse cells into metaclusters automatically, and thus results in an unbiased

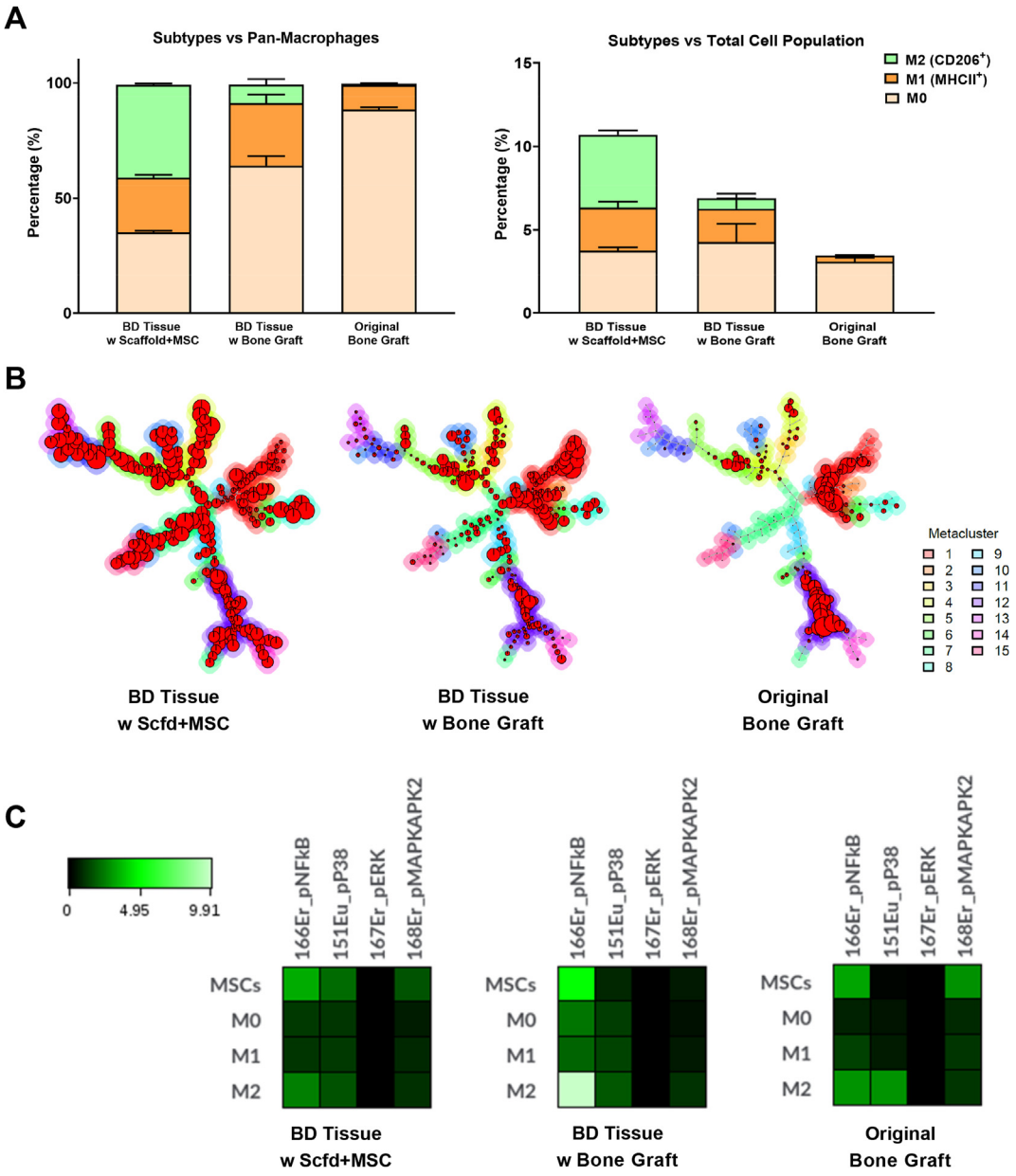

Fig. 5. Heterogeneity of macrophages. A) Different proportion of macrophage subtypes among three groups of samples. B) FlowSOM figures demonstrate the heterogeneity of macrophages among three groups. C) Activation of NF-κB signaling pathway in MSCs and M2 macrophages from the BD tissue containing bone graft.

clustering and classification of macrophages.

The FlowSOM analysis showed that the macrophage population in the "Original Bone Graft" group was mainly derived from 2 metaclusters (red & purple) (Fig. 5B, right). In the "BD Tissue w Bone Graft" group and the BD Tissue w Scaffold + MSC" group, the number of metaclusters progressively increased from 6 to 8 to 15, suggesting increasing diversity in macrophage phenotypes. The FlowSOM results reveal many subpopulations of macrophages (instead of just M1 and M2) within the bone defect sites, especially when transplanted with the scaffold plus MSCs. Considering many MSCs have been embedded into the scaffold in this group, this finding might suggest active crosstalk between MSCs and macrophages within the local niche at the bone defect site.

Next, we evaluated the activities of several major signaling pathways (including NF-κB, p38, ERK, and MAPK) among MSCs and macrophage subsets (Fig. 5C). We observed that in the defect containing bone graft, the activity of the NF-κB signaling pathway was dramatically elevated in both MSCs and M2 macrophages. This suggests that the pro-inflammatory microenvironment had not yet resolved. Bone healing begins with a stage of acute inflammation that lasts several days and then progresses to resolution and reparative stages in which acute inflammation subsides. We studied the tissues collected at the bone defect site at one-week post-operation #2. It is expected that the sites first become pro-inflammatory in the first a few days and then turn into an anti-inflammatory milieu after operation #2; this is on a back-drop of chronic inflammation in our model. When acute inflammation subsides, there is a change of polarization from M1 to M2 macrophage phenotype. However, persistence of upregulated NFkB reflects persistent adverse inflammatory processes which delay the resolution and reparative stages of bone healing.

The Composition of T Cells is Distinctive Between Bone Defect Tissues with Different Transplants, Demonstrating Stronger Inflammation Using the MSC plus Scaffold Therapy.

There are significant numbers of T cells in the bone defect tissues, however, the number of T cells in the "Original Bone Graft" group is small (Fig. 3A, center). This suggests that the majority of the T cells at the bone defect site transplanted with bone graft are recruited from the host mice, rather than from the original bone graft. This observation is confirmed by examining the CD90.2 biomarker that is only expressed in the host mice (Fig. 6A).

We performed FlowSOM analysis of the T-cell population identified using viSNE analysis. Although the proportions of T cells are similar between the "BD Tissue w Scaffold + MSC" group and the "BD Tissue w Bone Graft" group, FlowSOM results show distinct differences between groups (Fig. 6B). T cells from the "BD Tissue w Scaffold + MSC" group show higher level of phenotypic diversity than those from the "BD Tissue w Bone Graft" group; this finding is similar to what we observed in the macrophage population.

To further study the phenotypic diversity of the T cell population, individual T-cell subtypes, including helper T cells ($CD45^+$, $Ly6G^-$, $CD3^+$, $CD4^+$), cytotoxic T cells ($CD45^+$, $Ly6G^-$, $CD3^+$, $CD8^+$), and double-negative (DN) T cells ($CD45^+$, $Ly6G^-$, $CD3^+$, $CD4^-$, $CD8^-$) were evaluated (Fig. 6C). In the "BD Tissue w Scaffold + MSC" group, $CD4^+$ T cells form a major population and consist of about 68% of the total T-cell population whereas $CD8^+$ T cells consist of about 10%. Both of their proportions are significantly higher than those in the "BD Tissue w Bone Graft" group, which is about 10% for $CD4^+$ T cells and 2% for $CD8^+$ T cells, respectively. In contrast, the majority of the T-cell population in the "BD Tissue w Bone Graft" group is DN T cells (about 86%). Since most of the T cells (93%) are recruited to the bone defect site (Fig. 6A) and the peripheral T cells should mainly consist of $CD4^+$ T cells and $CD8^+$ T cells in a 2:1 ratio [52,53], it is interesting to observe such a high percentage of DN T cells in the bone defect site transplanted with the bone graft, but not with the scaffold plus MSCs.

DN T cells have been regarded as a strong suppressor of the alloreactive immune response during transplantation in both mice and humans [54–59]. A recent study has reported that the number of DN T cells is negatively correlated with the severity of the graft-versus-host disease (GvHD) in preclinical transplantation models and shows immunomodulatory potential by preventing pathological B cell responses in vivo [60]. These findings are consistent with our present findings, that in the "BD Tissue w Bone Graft" group, there are high percentages (approximately 86%) of DN T cells (Fig. 6C), and very rare B cells (<1%) (Fig. 3A, middle-left), whereas in the "BD Tissue w Scaffold + MSC" group there are low numbers (<20%) of DN T cells (Fig. 6C), but

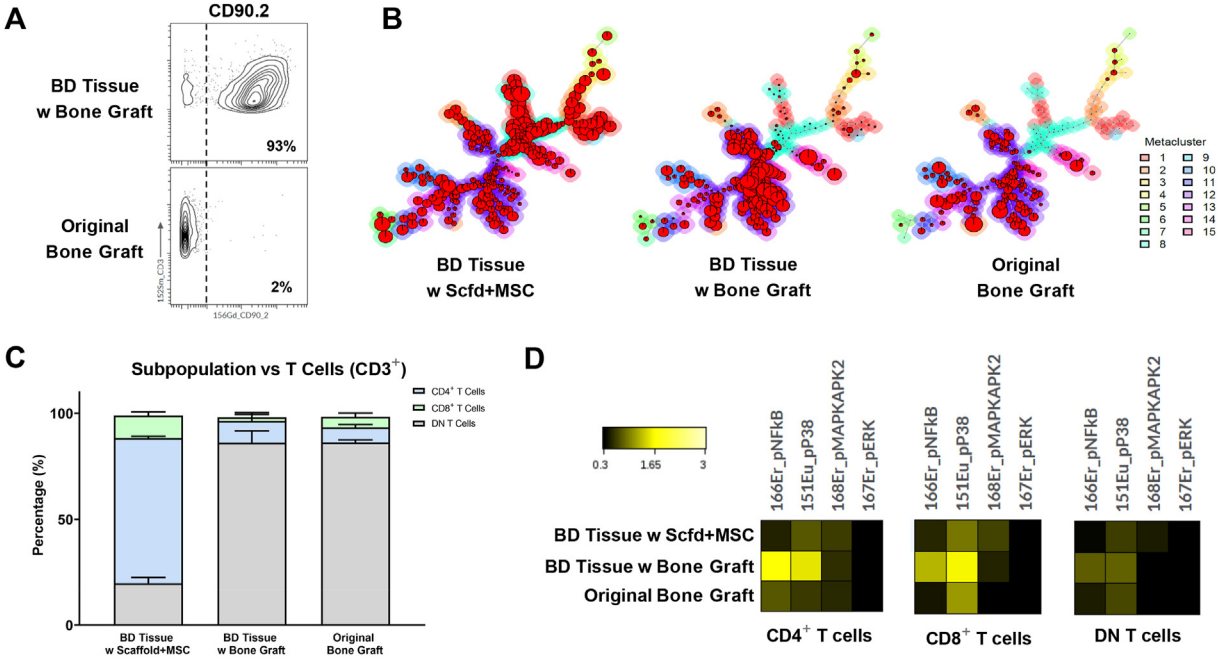

Fig. 6. The Composition of T Cells is Distinctively Different among Bone Defect Tissues with Different Transplants. A) CD90.2 expression level shows the originality of the T cells. B) FlowSOM analysis demarcates distinct T cell subsets among groups. C) Comparison of T-cell subpopulation in percentage. D) Heatmaps of functional markers in T-cell subtypes among groups.

significantly more B cells (~11%) (Fig. 3A, middle-left). Others have reported that DN T cells can modulate $CD4^+$ T cells' functionality by abrogating the mTOR signaling pathway and stimulating both NF-κB and p38 pathways [61]. This has also been observed in our studies (Fig. 6D). In the "BD Tissue w Bone Graft" group which has high level (~86%) of DN T cells (Fig. 6C), both NF-κB and p38 pathways are highly expressed in $CD4^+$ T cells and $CD8^+$ T cells, compared with the other two groups.

Taken together, the accumulation of DN T cells within the bone defect sites transplanted with bone graft, but not with the scaffold plus MSCs, might indicate a DN T cells-mediated inhibition of the alloreactive immune response could facilitate an improved clinical outcome in treating critical-size bone defect using bone graft versus scaffold plus MSCs.

4. Discussion

Critical-size bone defects remain a significant challenge and an unmet clinical need. Previously we and others have shown that after 4 weeks, a critical size bone defect with nonunion develops with this model. Our previous research [9] has shown promising enhancement of bone healing using local delivery of MSCs at time 0, during the acute inflammatory stage; however further research showed the efficacy of delivery of MSCs during the chronic inflammatory stage of nonunion was unsuccessful (unpublished data). We chose the time point of four weeks after the primary surgery during the chronic inflammatory stage of a nonunion, as potential therapies to achieve union at this time are an unmet clinical need. We investigated two reconstructive options for such defects: syngeneic (simulating autologous) bone grafting versus MSC-based therapy together with a supporting matrix [62,63] and revealed distinct cell compositions of tissues from bone defect sites treated with these two options. Both treatments show active recruitment of MSCs to the bone defect sites, but the macrophages and T cell populations are more diverse when the bone defect site is treated with the MSC-based therapy.

Autologous bone grafting is regarded as the gold standard for treating critical-size bone defects. Although autogenous grafts are effective, they often require an additional surgical site to harvest the bone graft (with potential surgical complications) and the amount of autologous bone may be limited in quantity and quality [2]. Although allogenic bone may be sufficient in quantity, it lacks viable cells and active growth factors and is incapable of inducing bone healing of critical size defects [3].

MSCbased therapy is a relatively new method for bone regeneration and has gained more attention in recent years [38–40, 64–70]. MSC-based therapy possesses multiple advantages over autologous bone grafting. First, MSC-based therapy is less invasive as it does not require an additional open wound to harvest bone graft, and therefore, decreases the risk of potential complications. Second, since the cells and the scaffolds are both scalable in vitro, MSC-based therapy is less likely to be constrained by the size and quantity of the implants to fill large bone defects. Third, once the process is optimized, MSC-based therapy may have the potential to regenerate bone even faster and more efficiently than autologous bone grafting.

Despite these potential advantages, MSC-based therapy is still not a first line treatment for obtaining union of critical size bone defects. To elucidate and differentiate the fundamental mechanisms of inducing bone healing for these two treatments and determine potential approaches for optimization of MSC-based therapy, we have designed three cohorts of experimental groups using a well-established murine critical-size bone femoral bone defect model. The first cohort demonstrates the natural biological state of the critical-size bone defect without any subsequent surgical intervention. The second cohort simulates the use of autologous bone grafting for treating critical-size bone defects. The third cohort examines the use of MSC-based therapy, where MSCs were carried by a novel scaffold and transplanted into the bone defect site to stimulate bone regeneration.

MSCbased therapy shows great potential but still requires significant improvements to achieve similar clinical outcomes compared with bone graft transplantation [71, 72]. Our results have revealed differences in the cellular compositions between transplanted bone graft and MSC-based therapy. By comparing these differences, we can adjust the MSC-based therapy to mimic the healing effect induced by bone graft. We also demonstrated that there is active recruitment of multiple cell types, including MSCs and other immune cells, to bone defect sites during the bone healing process. It is widely accepted that MSCs play a critical role during bone healing, as they are the progenitors of osteoblasts. However, constant communication between MSCs and other cell types collectively contribute to the process of bone formation.

Crosstalk between macrophages and MSCs has been studied extensively and has been shown to facilitate bone healing [73,74]. MSC-secreted growth factors can polarize macrophages from a pro-inflammatory M1 phenotype to an anti-inflammatory M2 phenotype [75,76], which in turn, facilitates bone healing. In this study, we went beyond the conventional classification of M1 and M2 macrophages and examined the overall heterogeneity status of the macrophage population via FlowSOM and observed a significantly higher heterogeneity in the defect with scaffold plus MSCs compared to the defect with transplanted bone graft. This reflected an elevated immunomodulatory activity at the bone defect site transplanted with scaffold plus MSCs.

MSCs also create a microenvironment that can suppress the proliferation of CD4+ and CD8+ T cells, while promoting the expansion of T regulatory cells [77, 78]. This suppression is especially prominent in the defect with transplanted bone graft, as we observed significantly less CD4+ and CD8+ T cells, and more DN T cells in the defect with transplanted bone graft compared to the defect with scaffold plus MSCs. As DN T cells have been widely reported to suppress alloreactive immune response during transplantation [54–59], this might contribute to better clinical outcomes by using bone graft as the transplants.

There are several limitations to our study. First, we have only included one scaffold group embedded with unaltered MSCs. While this typically represents current MSC-based therapy, gene-modified MSCs [9] or MSCs combined with nanoparticle-mediated growth factors (such as TGF-β) [79] may further enhance bone healing. This study is the first step in developing advanced MSC-based therapy, to achieve improve clinical outcomes compared with autologous bone graft procedures. Second, when designing the antibody panel for the CyTOF analysis in this study, we primarily focused on common phenotypic biomarkers and 4 major signaling pathways. As we gain further insights into the cell compositions and biological pathways in the healing callus using this model, further studies could focus on changes in different cellular biomarkers, relevant functional pathways, and gene-expression levels in the critical cell subtypes over time. Previous studies have shown that cellular crosstalk is integral to the bone healing process [73,74]. Although CyTOF can elucidate the key cells and mechanistic pathways that are important to bone healing, additional methods that explore complex cellular interactions will further expand our understanding of the processes of bone healing in a complex multi-cellular microenvironment.

In summary, traditional research methods, such as histomorphometry, immunohistochemistry, qPCR, flow cytometry, cell and organ culture and others have been used to elucidate the mechanisms underlying healing at bone defect sites. The current study using a new and cutting-edge methodology, namely CyTOF, provides a highly innovative perspective of the cellular composition, functionalities, and cell–cell interactions within bone defect sites early in the healing process. Our CyTOF results have systematically compared the cellular and immunomodulatory profiles among different interventions to obtain bone healing and have identified specific areas that warrant further exploration to improve MSC-based therapy for treating critical-size bone defects. Other novel methodologies are currently being implemented in our laboratory and by others to further understand the complexities of failed bone healing. This research area is critical to solving an unmet clinical need.

Funding/Support statement

This work was supported by NIH grants R01AR063717, R01AR073145, R35GM137936, and Ellenberg Chair in Surgery at Stanford.

Declaration of competing interest

The authors have no conflicts of interest relevant to this article.

Acknowledgements

We would like to thank Drs. Robert Negrin and Jeanette Baker for kindly sharing the gene-modified CD90.1 BALB/cByJ mice to support this study.

Appendix A. Supplementary data

Supplementary data to this article can be found online at https://doi.org/10.1016/j.jot.2022.05.010.

References

[1] Hak DJ, Fitzpatrick D, Bishop JA, Marsh JL, Tilp S, Schnettler R, et al. Delayed union and nonunions: epidemiology, clinical issues, and financial aspects. Injury 2014;45(Suppl 2):S3–7.
[2] Sohn HS, Oh JK. Review of bone graft and bone substitutes with an emphasis on fracture surgeries. Biomater Res 2019;23:9.
[3] Burchardt H. Biology of bone transplantation. Orthop Clin N Am 1987;18(2):187–96.
[4] Stoddart MJ, Hofmann S, Holnthoner W. Editorial: MSC signaling in regenerative medicine. Front Bioeng Biotechnol 2020;8:614561.
[5] Bunpetch V, Zhang ZY, Zhang X, Han S, Zongyou P, Wu H, et al. Strategies for MSC expansion and MSC-based microtissue for bone regeneration. Biomaterials 2019;196:67–79.
[6] Zha K, Sun Z, Yang Y, Chen M, Gao C, Fu L, et al. Recent developed strategies for enhancing chondrogenic differentiation of MSC: impact on MSC-based therapy for cartilage regeneration. Stem Cell Int 2021;2021:8830834.
[7] Khatri R, Petry SF, Linn T. Intrapancreatic MSC transplantation facilitates pancreatic islet regeneration. Stem Cell Res Ther 2021;12(1):121.
[8] Pumberger M, Qazi TH, Ehrentraut MC, Textor M, Kueper J, Stoltenburg-Didinger G, et al. Synthetic niche to modulate regenerative potential of MSCs and enhance skeletal muscle regeneration. Biomaterials 2016;99:95–108.
[9] Ueno M, Lo CW, Barati D, Conrad B, Lin T, Kohno Y, et al. Interleukin-4 overexpressing mesenchymal stem cells within gelatin-based microribbon hydrogels enhance bone healing in a murine long bone critical-size defect model. J Biomed Mater Res 2020;108(11):2240–50.
[10] Schmidt-Bleek K, Schell H, Schulz N, Hoff P, Perka C, Buttgereit F, et al. Inflammatory phase of bone healing initiates the regenerative healing cascade. Cell Tissue Res 2012;347(3):567–73.
[11] Lin T, Pajarinen J, Kohno Y, Huang JF, Maruyama M, Romero-Lopez M, et al. Trained murine mesenchymal stem cells have anti-inflammatory effect on macrophages, but defective regulation on T-cell proliferation. Faseb J 2019;33(3):4203–11.
[12] Pajarinen J, Lin T, Gibon E, Kohno Y, Maruyama M, Nathan K, et al. Mesenchymal stem cell-macrophage crosstalk and bone healing. Biomaterials 2019;196:80–9.
[13] Nathan K, Lu LY, Lin T, Pajarinen J, Jamsen E, Huang JF, et al. Precise immunomodulation of the M1 to M2 macrophage transition enhances mesenchymal stem cell osteogenesis and differs by sex. Bone Joint Res 2019;8(10):481–8.
[14] Romero-Lopez M, Li Z, Rhee C, Maruyama M, Pajarinen J, O'Donnell B, et al. Macrophage effects on mesenchymal stem cell osteogenesis in a three-dimensional in vitro bone model. Tissue Eng 2020;26(19–20):1099–111.
[15] Chow SK, Chim YN, Wang J, Zhang N, Wong RM, Tang N, et al. Vibration treatment modulates macrophage polarisation and enhances early inflammatory response in oestrogen-deficient osteoporotic-fracture healing. Eur Cell Mater 2019;38:228–45.
[16] Lin TH, Sato T, Barcay KR, Waters H, Loi F, Zhang R, et al. NF-kappaB decoy oligodeoxynucleotide enhanced osteogenesis in mesenchymal stem cells exposed to polyethylene particle. Tissue Eng 2015;21(5–6):875–83.
[17] Zhang N, Lo CW, Utsunomiya T, Maruyama M, Huang E, Rhee C, et al. PDGF-BB and IL-4 co-overexpression is a potential strategy to enhance mesenchymal stem cell-based bone regeneration. Stem Cell Res Ther 2021;12(1):40.
[18] Zhang N, Utsunomiya T, Lin T, Kohno Y, Ueno M, Maruyama M, et al. Mesenchymal stem cells and NF-κB sensing interleukin-4 over-expressing mesenchymal stem cells are equally effective in mitigating particle-associated chronic inflammatory bone loss in mice. Front Cell Dev Biol 2021:2906.
[19] Zwingenberger S, Niederlohmann E, Vater C, Rammelt S, Matthys R, Bernhardt R, et al. Establishment of a femoral critical-size bone defect model in immunodeficient mice. J Surg Res 2013;181(1):e7–14.
[20] M. Ueno, N. Zhang, H. Hirata, D. Barati, T. Utsunomiya, H. Shen, et al, Sex differences in mesenchymal stem cell therapy with gelatin-based microribbon hydrogels in a murine long bone critical-size defect model, Front Bioeng Biotechnol 972.
[21] Pierini A, Colonna L, Alvarez M, Schneidawind D, Nishikii H, Baker J, et al. Donor requirements for regulatory T cell suppression of murine graft-versus-host disease. J Immunol 2015;195(1):347–55.
[22] Conrad B, Han LH, Yang F. Gelatin-based microribbon hydrogels accelerate cartilage formation by mesenchymal stem cells in three dimensions. Tissue Eng 2018;24(21–22):1631–40.
[23] Han LH, Conrad B, Chung MT, Deveza L, Jiang X, Wang A, et al. Winner of the young investigator award of the society for biomaterials at the 10th world biomaterials congress, may 17-22, 2016, montreal QC, Canada: microribbon-based hydrogels accelerate stem cell-based bone regeneration in a mouse critical-size cranial defect model. J Biomed Mater Res 2016;104(6):1321–31.
[24] Gaudilliere B, Fragiadakis GK, Bruggner RV, Nicolau M, Finck R, Tingle M, et al. Clinical recovery from surgery correlates with single-cell immune signatures. Sci Transl Med 2014;6(255):255ra131.
[25] Spatz JM, Fulford MH, Tsai A, Gaudilliere D, Hedou J, Ganio E, et al. Human immune system adaptations to simulated microgravity revealed by single-cell mass cytometry. Sci Rep 2021;11(1):11872.
[26] Peterson LS, Hedou J, Ganio EA, Stelzer IA, Feyaerts D, Harbert E, et al. Single-cell analysis of the neonatal immune system Across the gestational age continuum. Front Immunol 2021;12:714090.
[27] Rosales C. Neutrophil: a cell with many roles in inflammation or several cell types? Front Physiol 2018;9:113.
[28] Butterfield TA, Best TM, Merrick MA. The dual roles of neutrophils and macrophages in inflammation: a critical balance between tissue damage and repair. J Athl Train 2006;41(4):457–65.
[29] Schlundt C, El Khassawna T, Serra A, Dienelt A, Wendler S, Schell H, et al. Macrophages in bone fracture healing: their essential role in endochondral ossification. Bone 2018;106:78–89.
[30] Wu AC, Raggatt LJ, Alexander KA, Pettit AR. Unraveling macrophage contributions to bone repair. BoneKEy Rep 2013;2:373.
[31] Banchereau J, Steinman RM. Dendritic cells and the control of immunity. Nature 1998;392(6673):245–52.
[32] Plekhova NG, Lyapun IN, Gnedenkov S, Sinebryukhov S, Mashtalyar D. The role of dendritic cells in bone loss and repair. 2018. Dendritic Cells, IntechOpen.
[33] Konnecke I, Serra A, El Khassawna T, Schlundt C, Schell H, Hauser A, et al. T and B cells participate in bone repair by infiltrating the fracture callus in a two-wave fashion. Bone 2014;64:155–65.
[34] Almeida CR, Vasconcelos DP, Goncalves RM, Barbosa MA. Enhanced mesenchymal stromal cell recruitment via natural killer cells by incorporation of inflammatory signals in biomaterials. J R Soc Interface 2012;9(67):261–71.
[35] Petri RM, Hackel A, Hahnel K, Dumitru CA, Bruderek K, Flohe SB, et al. Activated tissue-resident mesenchymal stromal cells regulate natural killer cell immune and tissue-regenerative function. Stem Cell Rep 2017;9(3):985–98.
[36] Hirata H, Zhang N, Ueno M, Barati D, Kushioka J, Shen H, et al. Ageing attenuates bone healing by mesenchymal stem cells in a microribbon hydrogel with a murine long bone critical-size defect model. Immun Ageing 2022;19(1):14.
[37] Ueno M, Zhang N, Hirata H, Barati D, Utsunomiya T, Shen H, et al. Sex differences in mesenchymal stem cell therapy with gelatin-based microribbon hydrogels in a murine long bone critical-size defect model. Front Bioeng Biotechnol 2021;9:755964.
[38] Klontzas ME, Kenanidis EI, Heliotis M, Tsiridis E, Mantalaris A. Bone and cartilage regeneration with the use of umbilical cord mesenchymal stem cells. Expet Opin Biol Ther 2015;15(11):1541–52.
[39] Gomez-Barrena E, Rosset P, Lozano D, Stanovici J, Ermthaller C, Gerbhard F. Bone fracture healing: cell therapy in delayed unions and nonunions. Bone 2015;70:93–101.
[40] Perez JR, Kouroupis D, Li DJ, Best TM, Kaplan L, Correa D. Tissue engineering and cell-based therapies for fractures and bone defects. Front Bioeng Biotechnol 2018;6:105.
[41] Pittenger MF, Mackay AM, Beck SC, Jaiswal RK, Douglas R, Mosca JD, et al. Multilineage potential of adult human mesenchymal stem cells. Science 1999;284(5411):143–7.
[42] Alvarez-Viejo M, Menendez-Menendez Y, Blanco-Gelaz MA, Ferrero-Gutierrez A, Fernandez-Rodriguez MA, Gala J, et al. Quantifying mesenchymal stem cells in the mononuclear cell fraction of bone marrow samples obtained for cell therapy. Transplant Proc 2013;45(1):434–9.
[43] Maruyama M, Rhee C, Utsunomiya T, Zhang N, Ueno M, Yao Z, et al. Modulation of the inflammatory response and bone healing. Front Endocrinol 2020;11:386.
[44] Murray PJ. Macrophage polarization. Annu Rev Physiol 2017;79:541–66.
[45] Zhou Y, Yoshida S, Kubo Y, Yoshimura T, Kobayashi Y, Nakama T, et al. Different distributions of M1 and M2 macrophages in a mouse model of laser-induced choroidal neovascularization. Mol Med Rep 2017;15(6):3949–56.
[46] Mills CD. Anatomy of a discovery: m1 and m2 macrophages. Front Immunol 2015;6:212.
[47] Mantovani A, Sica A, Sozzani S, Allavena P, Vecchi A, Locati M. The chemokine system in diverse forms of macrophage activation and polarization. Trends Immunol 2004;25(12):677–86.
[48] Duluc D, Delneste Y, Tan F, Moles MP, Grimaud L, Lenoir J, et al. Tumor-associated leukemia inhibitory factor and IL-6 skew monocyte differentiation into tumor-associated macrophage-like cells. Blood 2007;110(13):4319–30.
[49] Wang LX, Zhang SX, Wu HJ, Rong XL, Guo J. M2b macrophage polarization and its roles in diseases. J Leukoc Biol 2019;106(2):345–58.

[50] Roszer T. Understanding the mysterious M2 macrophage through activation markers and effector mechanisms. Mediat Inflamm 2015;2015:816460.
[51] Kudlik G, Hegyi B, Czibula A, Monostori E, Buday L, Uher F. Mesenchymal stem cells promote macrophage polarization toward M2b-like cells. Exp Cell Res 2016; 348(1):36–45.
[52] Kleiveland CR. Peripheral blood mononuclear cells. In: Verhoeckx K, Cotter P, Lopez-Exposito I, Kleiveland C, Lea T, Mackie A, et al., editors. The Impact of Food Bioactives on Health: in vitro and ex vivo models. Cham: CH); 2015. p. 161–7.
[53] Juvet SC, Zhang L. Double negative regulatory T cells in transplantation and autoimmunity: recent progress and future directions. J Mol Cell Biol 2012;4(1): 48–58.
[54] Voelkl S, Gary R, Mackensen A. Characterization of the immunoregulatory function of human TCR-alphabeta+ CD4- CD8- double-negative T cells. Eur J Immunol 2011; 41(3):739–48.
[55] Zhang Z, Yang L, Young KJ, Zhang L. Suppression of alloimmune responses in vitro and in vivo by CD3(+)CD8(-)CD4(-)alphabeta(+) regulatory T cells. Transplant Proc 2001;33(1–2):84–5.
[56] Zhang ZX, Yang L, Young KJ, DuTemple B, Zhang L. Identification of a previously unknown antigen-specific regulatory T cell and its mechanism of suppression. Nat Med 2000;6(7):782–9.
[57] Chen W, Ford MS, Young KJ, Zhang L. The role and mechanisms of double negative regulatory T cells in the suppression of immune responses. Cell Mol Immunol 2004; 1(5):328–35.
[58] Young KJ, DuTemple B, Phillips MJ, Zhang L. Inhibition of graft-versus-host disease by double-negative regulatory T cells. J Immunol 2003;171(1):134–41.
[59] McIver Z, Serio B, Dunbar A, O'Keefe CL, Powers J, Wlodarski M, et al. Double-negative regulatory T cells induce allotolerance when expanded after allogeneic haematopoietic stem cell transplantation. Br J Haematol 2008;141(2):170–8.
[60] Hillhouse EE, Thiant S, Moutuou MM, Lombard-Vadnais F, Parat R, Delisle JS, et al. Double-negative T cell levels correlate with chronic graft-versus-host disease severity. Biol Blood Marrow Transplant 2019;25(1):19–25.
[61] Haug T, Aigner M, Peuser MM, Strobl CD, Hildner K, Mougiakakos D, et al. Human double-negative regulatory T-cells induce a metabolic and functional switch in effector T-cells by suppressing mTOR activity. Front Immunol 2019;10:883.
[62] McClure PK, Abouei M, Conway JD. Reconstructive options for tibial bone defects. J Am Acad Orthop Surg; 2021. p. 901–9.
[63] Kumar P, Vinitha B, Fathima G. Bone grafts in dentistry. J Pharm BioAllied Sci 2013;5(Suppl 1):S125–7.
[64] Park JS, Suryaprakash S, Lao YH, Leong KW. Engineering mesenchymal stem cells for regenerative medicine and drug delivery. Methods 2015;84:3–16.
[65] Asatrian G, Pham D, Hardy WR, James AW, Peault B. Stem cell technology for bone regeneration: current status and potential applications. Stem Cells Cloning 2015;8: 39–48.
[66] Horwitz EM, Prockop DJ, Fitzpatrick LA, Koo WW, Gordon PL, Neel M, et al. Transplantability and therapeutic effects of bone marrow-derived mesenchymal cells in children with osteogenesis imperfecta. Nat Med 1999;5(3):309–13.
[67] Horwitz EM, Gordon PL, Koo WK, Marx JC, Neel MD, McNall RY, et al. Isolated allogeneic bone marrow-derived mesenchymal cells engraft and stimulate growth in children with osteogenesis imperfecta: implications for cell therapy of bone. Proc Natl Acad Sci U S A 2002;99(13):8932–7.
[68] Griffin M, Iqbal SA, Bayat A. Exploring the application of mesenchymal stem cells in bone repair and regeneration. J Bone Joint Surg Br 2011;93(4):427–34.
[69] Ismail HD, Phedy P, Kholinne E, Djaja YP, Kusnadi Y, Merlina M, et al. Mesenchymal stem cell implantation in atrophic nonunion of the long bones: a translational study. Bone Joint Res 2016;5(7):287–93.
[70] Jin YZ, Lee JH. Mesenchymal stem cell therapy for bone regeneration. Clin Orthop Surg 2018;10(3):271–8.
[71] Marcacci M, Kon E, Moukhachev V, Lavroukov A, Kutepov S, Quarto R, et al. Stem cells associated with macroporous bioceramics for long bone repair: 6- to 7-year outcome of a pilot clinical study. Tissue Eng 2007;13(5):947–55.
[72] Quarto R, Mastrogiacomo M, Cancedda R, Kutepov SM, Mukhachev V, Lavroukov A, et al. Repair of large bone defects with the use of autologous bone marrow stromal cells. N Engl J Med 2001;344(5):385–6.
[73] Shin RL, Lee CW, Shen OY, Xu H, Lee OK. The crosstalk between mesenchymal stem cells and macrophages in bone regeneration: a systematic review. Stem Cell Int 2021;2021:8835156.
[74] Carty F, Mahon BP, English K. The influence of macrophages on mesenchymal stromal cell therapy: passive or aggressive agents? Clin Exp Immunol 2017;188(1): 1–11.
[75] Luz-Crawford P, Djouad F, Toupet K, Bony C, Franquesa M, Hoogduijn MJ, et al. Mesenchymal stem cell-derived interleukin 1 receptor antagonist promotes macrophage polarization and inhibits B cell differentiation. Stem Cell 2016;34(2): 483–92.
[76] Braza F, Dirou S, Forest V, Sauzeau V, Hassoun D, Chesne J, et al. Mesenchymal stem cells induce suppressive macrophages through phagocytosis in a mouse model of asthma. Stem Cell 2016;34(7):1836–45.
[77] Negi N, Griffin MD. Effects of mesenchymal stromal cells on regulatory T cells: current understanding and clinical relevance. Stem Cell 2020;38(5):596–605.
[78] Di Ianni M, Del Papa B, De Ioanni M, Moretti L, Bonifacio E, Cecchini D, et al. Mesenchymal cells recruit and regulate T regulatory cells. Exp Hematol 2008;36(3): 309–18.
[79] Barati D, Gegg C, Yang F. Nanoparticle-mediated TGF-beta release from microribbon-based hydrogels accelerates stem cell-based cartilage formation in vivo. Ann Biomed Eng 2020;48(7):1971–81.